ISSN (e): 2250 – 3005 || Volume, 13 || Issue, 1|| Jan. - Feb. – 2023 ||
International Journal of Computational Engineering Research (IJCER)

A Brief Overview of a Simple and Efficient Windshear Doppler-Radar Detector for Aircraft Early Warning

Christos Papachristos
Cloud Signals P.C.
3 Trebesinas Str., GR 16673, Voula
Athens, GREECE

Panagiotis J. Papakanellos
Department of Aeronautical Sciences
Hellenic Air Force Academy
Dekeleia Air Force Base
GR 13671, Dekeleia, Athens, GREECE

Abstract– *This paper contains a brief overview of how a pulse Doppler radar can be used as a predictive windshear system. It is well known that windshear can be hazardous for aircraft flying at low altitudes. An airborne pulse Doppler (weather) radar is capable of warning the pilot in reasonable time before hazardous weather is encountered. The radar transmits a train of pulses, backscattered reflections of which can provide information about the nature of weather targets and turbulence. The return signal is filtered so as to remove unwanted returns and processed directly in the time domain in order to obtain fast and accurate estimates for the mean and variance values of the windshear velocity spectrum. Numerous tests have been conducted to assess the computational cost and the accuracy of the pertinent estimations under adverse conditions. The estimators at hand have been fed with real data and proved capable of providing fast and accurate results for windshear occurrence.*

Index Terms—*Pulse Doppler Radar, Pulse-Pair Processing, Weather Radar, Windshear Detection*

Date of Submission: 26-12-2022 Date of acceptance: 06-01-2023

I. Introduction

Since the late 1970s, low-altitude windshear (often called a microburst) has become recognized as a significant possible hazard to aircraft during takeoff and landing, which can be detected by ground and airborne Doppler radars; significant early works on this subject include [1-10] and several others cited therein. The term microburst was first used by Fujita to describe a rapid downflow of air that upon impacting the ground forms a horizontal outflow extending less than 4 km in diameter [2]. Beginning at ranges nearest to the aircraft, the windspeed has a large negative value in the headwind, reducing to zero at the heart of the downdraft, and reaches a large positive value in the tailwind [7]. This characteristic change of windspeed can be detected using algorithms to estimate the mean and variance of the power spectral density of the return signal associated with the Doppler spectrum of the windshear. Related topics and processing techniques have remained of interest through the years until nowadays [11-16].

At this point, it is worth mentioning that modern aircraft carry weather radars with the capability to detect windshear events ahead of the aircraft (e.g., see [17-21]). This equipment is often referred to as Predictive Windshear System (PWS). Due to the nature of windshear turbulence, the time window in which the pilot can take actions to minimize the associated danger is not larger than a few seconds. Therefore, possible savings in the execution time of the PWS underlying algorithm are of critical importance for its adequacy, effectiveness, and applicability. The present work reviews windshear detection principles and techniques, and examines different estimators for identifying windshear turbulence from weather returns, which are compared from the aspect of the associated computational cost. To this end, cost functions are provided for three popular processing strategies, so as to proceed to a comparison on a fair and solid basis. Furthermore, dummy and real data are processed, and the accuracy of the estimations is examined and discussed. Finally, a few concluding remarks are outlined. Though no significant novelty is introduced herein, the aforesaid cost functions and the ensuing

comparisons are new. Moreover, the attempted overview can serve as a compact retrospective for avionics students and engineers.

Windshear Detection Principles and Techniques

In conventional radar nomenclature [22-25], a positive frequency shift in the return signal indicates an approaching target. After demodulated, the return signal yields a discrete sequence of complex samples (one per pulse). By passing this sequence through a low-pass filter, a baseband sequence is created, the so-called IQ one, which contains the pertinent in-phase and quadrature-phase components (from which the signal can be divided up into its real and imaginary parts). In general, a zero Doppler shift indicates a stationary target; however, for a moving radar platform (e.g., airborne radar), stationary objects have a relative velocity with respect to the radar. In order to center the returns from stationary objects (such as ground clutter) at zero, the demodulation frequency depends on the velocity of the aircraft. The next step of the signal-processing chain is to filter unwanted returns. One method of clutter rejection consists in the implementation of an ideal filter in the frequency domain by computing the discrete Fourier transform (DFT) of the return sequence and then simply zeroing out the signal power levels at (and near) zero Doppler [23]. Another popular clutter rejection technique is the use of a band-stop filter, which has a narrow notch at zero Doppler [23]. This method is used hereinafter by employing a second-order Butterworth filter with a normalized cut-off (notch) width between $\pm\pi/10$.

With regard to the extraction of spectral parameters, the majority of processors use DFT spectral windowing to obtain the Doppler spectrum from the time series of the return signal. Another processing strategy utilizes autoregressive (AR) spectral estimates instead of DFT windowing [9]. The general approach is to fit an AR model to the time series and generate a spectrum from the AR coefficients. Both these approaches can yield acceptable estimates, but at the expense of a quite large amount of computational cost/time. Alternatively, one can obtain fundamental spectral characteristics like mean and variance directly from the time series. This technique has been proposed by Rummler in 1968 and has been dubbed pulse-pair processing (PPP), since the computation requires two pulses (i.e., two consecutive returns from the same target) [3].

The superiority of PPP in terms of computational requirements can be seen from the number of operations required by a low-level code—which has been developed in C—as a function of the number of samples processed N. The computational cost of a processing implementation using the fast Fourier transform (FFT), including the overhead associated with second-order Butterworth filtering for clutter rejection, is approximately given by (1) below. For an AR model of order p, the computational cost is roughly given by (2) [6]

$$C_{\mathrm{FFT}} \approx 10N\log_2 N + 22N \tag{1}$$

$$C_{\mathrm{AR}} \approx (p+22)N + 10(p+2)\log_2 N + 6p^2 \tag{2}$$

On the other hand, in the case of the PPP combined with the aforesaid Butterworth filter, the mean and variance estimates are associated with computational cost as low as

$$C_{\mathrm{PPP}} \approx 26N \tag{3}$$

For $N=128$, one obtains $C_{\mathrm{FFT}} \approx 11776$, $C_{\mathrm{AR}} \approx 14296$ for an AR model of order $p=30$, and $C_{\mathrm{PPP}} \approx 3328$. Clearly, C_{PPP} is much smaller than both C_{FFT} and C_{AR} in this indicative case (namely, $C_{\mathrm{PPP}}/C_{\mathrm{FFT}} \approx 0.28$ and $C_{\mathrm{PPP}}/C_{\mathrm{AR}} \approx 0.23$), which is also true for all practical purposes. This big difference in the computational cost and the associated processing time can be proved valuable in real-time PWS applications. To illustrate the differences between the different schemes considered herein, Fig. 1 exhibits the results of (1)-(3) as a function of N.

In order to complete the PPP scheme for windshear detection, it is necessary to define a measure of the severity of a microburst in terms of its performance decreasing effect on an aircraft flying through the event. Two methods are commonly in use: namely, the 'S' curve signature that is formed from the horizontal component of windspeed versus range plot [2], and the 'F' factor, which is an aircraft independent measure of the severity of the windfield [2]. These topics are beyond the scope of the present work and are not discussed further.

Mean and Variance Estimations in the Time Domain

The radial velocity v due to Doppler shift of weather returns can be estimated (directly in the time domain) from the signal autocorrelation function. This technique is based on the calculation of the complex autocorrelation function starting from N successive complex samples of the return signal in a range cell

(division between transmitted and received pulse) with the proviso that its spectrum is symmetric. When the spectrum is asymmetric, this estimator is not strictly rigorous; however, the ensuing error is small and can be tolerated in most cases.

The aforesaid autocorrelation function $R(T_s)$ is related to the power spectral density $S(f)$ of the return signal, as follows

$$R(T_s) = e^{j2\pi f_d T_s} \int_{-\frac{1}{2T_s}}^{\frac{1}{2T_s}} S(f) e^{j2\pi(f-f_d)T_s}\, df \tag{4}$$

where T_s is the pulse repetition period and f_d is the Doppler frequency shift. When the spectrum is even around f_d, the integral on the right-hand side of (4) is real. Then, one readily obtains

$$f_d = \frac{1}{2\pi T_s} \tan^{-1}\left(\frac{\mathrm{Im}\{R(T_s)\}}{\mathrm{Re}\{R(T_s)\}}\right) \tag{5}$$

An estimate of $R(T_s)$ can be obtained from successive pulse pairs (or IQ pairs) directly from the time-domain signal samples [3]

$$\widetilde{R}(T_s) = \frac{1}{N}\sum_{n=0}^{N-2} Z_{n+1} Z_n^* \tag{6}$$

where $Z_n = I_n + jQ_n$ ($n = 0,1,2,...,N-1$) denotes the complex sample of the received signal and $Z_n^* = I_n - jQ_n$ is its complex conjugate.

From the preceding, an estimator for the mean radial velocity can be expressed as [4]

$$\widetilde{v} = -\frac{\lambda}{4\pi T_s} \mathrm{Arg}\{\widetilde{R}(T_s)\} \tag{7}$$

where λ is the wavelength and the function $\mathrm{Arg}\{\cdot\}$ returns the argument between $-\pi$ and π. The negative sign signifies that positive Doppler shifts yield negative velocities.

Special care should be taken to ensure that the spectrum $S(f)$ has components that do not exceed the Nyquist limits $\pm 1/(2T_s)$. If they do, these components are undersampled and the resulting mean frequency estimation is a biased estimation of the true mean (due to unwanted aliasing effects). However, even in this case, the argument of $\widetilde{R}(T_s)$ still yields the mean frequency to within an uncertainty equal to a multiple of the Nyquist interval.

Velocity spectrum variance σ_v^2 can also be calculated directly in the time domain using the magnitude of the autocorrelation estimate already calculated for radial velocity. The assumptions made, however, result in a valid estimate in cases of weather signals with symmetric spectral density (e.g., Gaussian) [3]. To this end, the pertinent formula for the standard deviation $\widetilde{\sigma}_v$ is [7]

$$\widetilde{\sigma}_v = \frac{\lambda}{2\sqrt{2}\pi T_s} \left| \ln \frac{\widetilde{S}}{\left|\widetilde{R}(T_s)\right|} \right|^{1/2} \mathrm{sgn}\left(\ln \frac{\widetilde{S}}{\left|\widetilde{R}(T_s)\right|} \right) \tag{8}$$

where $\widetilde{S}$ is the estimated average power return, given by

$$\widetilde{S} = \frac{1}{N}\sum_{n=0}^{N-1}|Z_n|^2 \tag{9}$$

Since $\widetilde{S}$ and $\widetilde{R}(T_s)$ are estimates, it is possible for the logarithm involved in (8) to become negative (namely, for narrow spectrum widths and low signal levels). The signum function $\mathrm{sgn}(\cdot)$ above tags these negative values, so as to neglect them without much risk to actually overlook a microburst.

As discussed above, the time-domain implementation of the PPP scheme has the advantage of being (significantly) more computationally efficient than DFT/FFT-based techniques. DFT/FFT-based estimators of spectral mean and variance can give better results than the PPP scheme, but only under conditions of high signal-to-noise ratios (SNRs) (and not near the Nyquist limits). On the other hand, AR modeling eliminates the problem of spectral leakage, as it does not force the sequence to be zero-valued outside the range of the data. However, the AR approach may not always be well suited to the problem, as it often requires high-order models to represent the process, which are computationally intensive and overall time-consuming.

II. Results

The PPP scheme discussed so far was first tested using IQ samples coming from artificial Gaussian Doppler spectra of various means and variances. The estimations obtained were very accurate for spectra of narrow widths with variance values between 1 and 10 $\mathrm{m^2 s^{-2}}$, and for mean windspeed values close to zero. For mean values close to the ambiguous limits, the estimations became worse, but often within acceptable limits. When spectra of large widths occurred (i.e., for variance values between 100 and 200 $\mathrm{m^2 s^{-2}}$), the estimation of mean windspeed was again very accurate for mean values between 0 and 10 $\mathrm{ms^{-1}}$. For windspeed values higher than 10 $\mathrm{ms^{-1}}$, the estimations were found to deviate significantly from the true values. However, spectra of such high values of mean and variance do not represent weather returns, but clutter reflections; thus, the accuracy of their spectrum estimations is not of any interest. For spectra that usually represent weather returns, the estimations were indeed found to be very accurate for standard deviation values up to 12 $\mathrm{ms^{-1}}$.

Indicative numerical results that illustrate the accuracy of the PPP scheme for windshear detection are shown Figs. 2 and 3. By keeping the velocity mean of the input spectrum equal to zero and varying the spectrum width, it is possible to obtain an indication of the accuracy in the estimation of the standard deviation $\widetilde{\sigma}_v$. This is demonstrated in Fig. 2. Furthermore, Fig. 3 shows the estimated values of velocity mean $\widetilde{v}$ and the corresponding widths $\widetilde{\sigma}_v$ when facing a spectrum of variance equal to 1 $\mathrm{m^2 s^{-2}}$. Obviously, very accurate estimations are possible in both cases. As a quantitative proof for this statement, one can compute the absolute percentage differences between true and estimated values. The average percentage error for the standard deviation values plotted in Fig. 2 is approximately 2%, whereas the corresponding error for the mean values plotted in Fig. 3 is not larger than 0.6%. As already pointed out, small discrepancies between true and estimated values were also found for spectra of variance up to 10 $\mathrm{m^2 s^{-2}}$.

It is worth stressing that the SNR of the return does not make any significant difference in the estimation of the mean. In fact, as successive samples are statistically independent, the error due to noise is zero on average. With regard to the estimation of the spectral width, it deviates significantly from the true value for low SNR values. Nevertheless, the accuracy becomes acceptable when SNR roughly exceeds 15-16 dB. This can be deduced from Fig. 4. White noise does not bias the estimated mean windspeed, as long as it has a constant power density over the frequency spectrum and, therefore, does not weight any particular frequencies.

Next, the PPP scheme under study was fed with real data provided by the 'Antenna and Microwave Research Branch', NASA Langley Research Center, USA. This set of data was produced by flight experiments performed in the area of Orlando under the NASA/FAA Windshear Program and belong to the recorded weather frame 970 consisting of 128 IQ pairs for each of 91 range cells. The shape of the microburst revealed after processing is shown in Fig. 5. The center (or core) representing the downdraft of the microburst is situated at range cell 33 from the aircraft. This is also the point when the headwind becomes tailwind. The rapid loss of altitude caused by the downdraft and the ensuing loss of aircraft altitude and speed due to the tailwind can bring the aircraft too close to the ground with too little kinetic energy to escape a crash. The range cell 33 corresponds to about 4752 m from the aircraft at the moment of detection. From Fig. 5, one can distinguish the large windspeed variation between range cells 70 to 90. These spikes are probably due to urban clutter at this location around the area of Orlando, and were not filtered by the Butterworth filter (at least not completely) since not all of them were situated around zero Doppler frequency.

III. Conclusion

An assessment study was conducted to evaluate the speed and accuracy performance of airborne pulse Doppler radars to detect hazardous microburst windshear. Towards this goal, return signals were filtered so as to remove unwanted returns and processed directly in the time domain, in order to yield fast and accurate estimates for the mean and variance values of the windshear spectrum.

Numerous computer simulations involving indicative benchmark cases and realistic weather returns (based on real data) were ran to test processing strategies that can be used for detection and to reveal the efficiency of the PPP scheme, which indeed provided fast and accurate spectral estimates that can be utilized for rapid and trustworthy windshear detection. Such a processing unit can be readily incorporated into airborne weather radars. To justify the use of the aforesaid approach against others, a computational cost comparison has been conducted and revealed that the PPP-based detector can run notably faster than other popular techniques without notable accuracy loss.

Acknowledgment

The authors would like to thank S. D. Harrah for providing real data from the ‘Antenna and Microwave Research Branch’, NASA Langley Research Center. The authors are also grateful to Ass. Prof. P. Louka of the Hellenic Air Force Academy, as well as to B1 Aircraft Engineer S. Marinakis, for valuable suggestions and comments.

References

[1]. E. M. Bracalente, C. L. Britt, W. R. Jones, “Airborne Doppler Radar Detection of Low Altitude Windshear,” AIAA Conference on Sensor and Measurement, Atlanta, Sep. 1988.
[2]. J. Evans and D. Turnbull, “Development of an Automated Windshear Detection System using Doppler Weather Radar,” Proceedings of the IEEE, Vol. 77, No. 11, pp. 1661-1673, 1989.
[3]. E. G. Baxa, Jr., and J. Lee, “The Pulse-Pair Algorithm as a Robust Estimator of Turbulent Weather Spectral Parameters Using Airborne Pulse Doppler Radar,” NASA CR-4382, Jul. 1991.
[4]. E. G. Baxa, Jr., “Airborne Pulsed Doppler Radar Detection of Low-Altitude Windshear—A Signal Processing Problem,” Digital Signal Processing, Vol. 1, No. 4, pp. 186-197, Oct. 1991.
[5]. E. G. Baxa, Jr., “Signal Processing for Airborne Doppler Radar Detection of Hazardous Windshear as Applied to NASA 1991 Radar Flight Experimental Data,” 4th CMTAW Meeting, Clemson University, Apr. 1992.
[6]. D. D. Aalfs, “Real-Time Processing of Radar Return on a Parallel Computer,” NASA CR-4456, Aug. 1992.
[7]. M. W. Kunkel, “Spectrum Modal Analysis for the Detection of Low-Altitude Windshear With Airborne Doppler Radar,” NASA CR-4457, Aug. 1992.
[8]. E. G. Baxa, Jr., “Windshear Detection Radar Signal Processing Studies—Final Report,” Technical Report No. 18, Radar Systems Laboratory, Clemson University, 1993.
[9]. D. D. Aalfs, E. G. Baxa, Jr., and E. M. Bracalente, “Signal Processing Aspects of Windshear Detection,” Microwave Journal, Vol. 36, No. 9, pp. 76-96, 1993.
[10]. F. H. Proctor, E. M. Bracalente, S. D. Harrah, G. F. Switzer, and C. L. Britt, “Simulation of the 1994 Charlotte Microburst with Look-Ahead Windshear Radar,” 27th Conference on Radar Meteorology, pp. 530-532, 1995.
[11]. L. A. Justena, G. Teschkea, and V. Lehmannb, “Wavelet-Based Methods for Clutter Removal from Radar Wind Profiler Data,” Wavelet Applications in Industrial Processing, Proceedings of SPIE, Vol. 5266, 2004.
[12]. V. I. Pokrovsky, V. V. Belkin, and F. J. Yanovsky, “Airborne Weather Radar for Windshear Detection,” 18th International Conference on Applied Electromagnetics and Communications, pp. 1-3, 2005.
[13]. M. Lagha and M. Bensebti, “Performances Comparison of Pulse-Pair and 2-Step Prediction Algorithms for the Doppler Spectrum Estimation,” Multidimensional Systems and Signal Processing, Vol. 19, pp. 257-265, 2008.
[14]. Y. Fan, R. Wu, Z. Meng, Z. Su, X. Lu, R. Wu, and J. Huang, “Wind Shear Signal Simulation of the Airborne Weather Radar,” IEEE Radar Conference, pp. 710-713, 2011.
[15]. M. Lagha, M. Tikhemirine, S. Bergheul, T. Rezoug, and M. Bettayeb, “Performance Comparison of Pulse-Pair and Wavelets Methods for the Pulse Doppler Weather Radar Spectrum,” HAL-00663005, 2012.
[16]. J. Y. N. Cho, “Enhanced Signal Processing Algorithms for the ASR-9 Weather Systems Processor,” Journal of Atmospheric and Oceanic Technology, Vol. 32, pp. 1847-1859, 2015.
[17]. FSF ALAR Briefing Note 5.4—Wind Shear, Flight Safety Foundation, Flight Safety Digest, pp. 111-116, Aug.-Nov. 2000.
[18]. D. Smith, “The Past, Present, and Future of Airborne Weather Radar,” Avionics News, pp. 42-44, Feb. 2006.
[19]. MMEL Policy Letter (PL) 67, Revision 4, “Windshear Warning and Flight Guidance System (RWS), Windshear Detection and Avoidance System (PWS),” Federal Aviation Administration, 2012.
[20]. L. Nguyen, “Technical Standard Order Authorization and Airworthiness Approval Considerations for Aircraft Weather Radar Systems,” 31st Digital Avionics Systems Conference, Oct. 2012.
[21]. AC 20-182A, “Airworthiness Approval for Aircraft Weather Radar Systems,” Federal Aviation Administration, 2016.
[22]. E. A. Robinson, Statistical Communication and Detection with a Special Reference to Digital Data Processing of Radar and Seismic Signals. Griffin, 1967.
[23]. G. V. Morris, Airborne Pulsed Doppler Radar. Artech House, 1988.
[24]. G. W. Stimson, Introduction to Airborne Radar, Second Edition. Scitech, 1998.
[25]. B.-C. Wang, Digital Signal Processing Techniques and Applications in Radar Image Processing. Wiley, 2008.

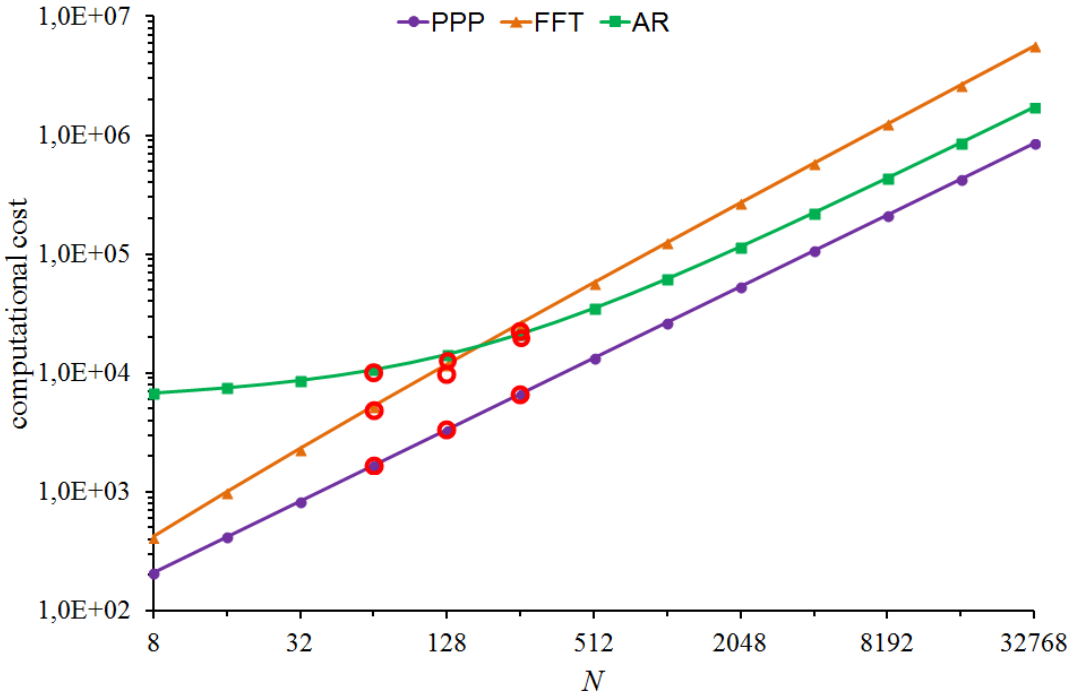

Fig. 1. Comparative plot of the computational cost of windshear detection schemes as a function of N .

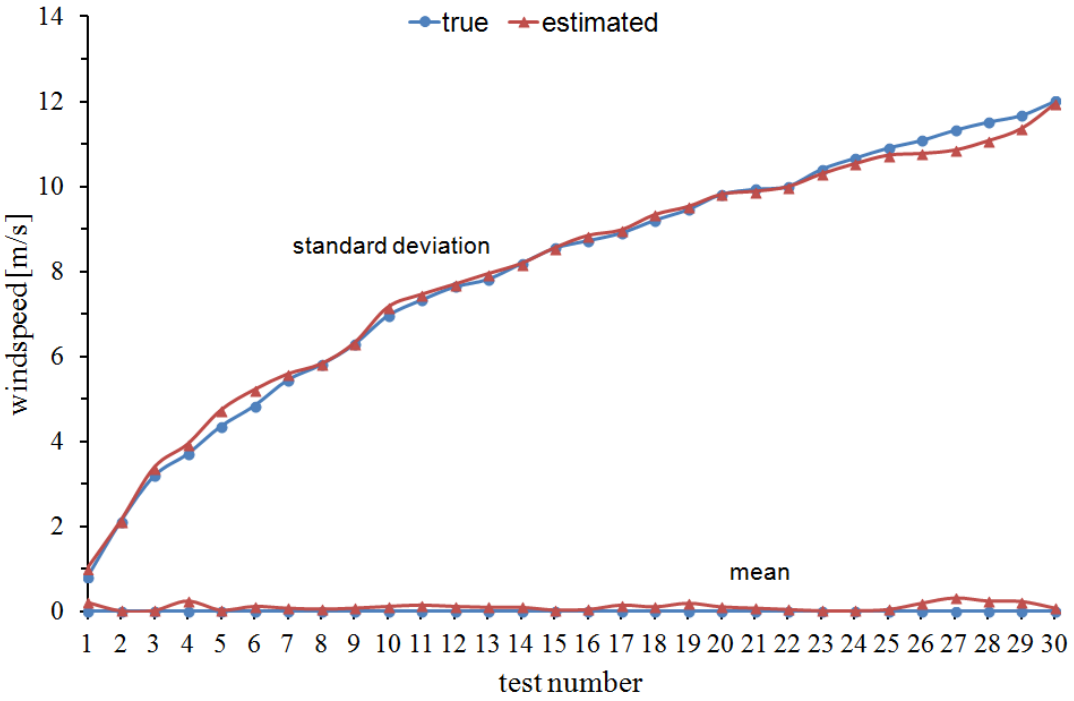

Fig. 2. Estimated mean $\tilde{v}$ and standard deviation $\tilde{\sigma}_v$, as obtained from the PPP scheme, for an input spectrum with true velocity mean equal to zero and varying width. The true values are also shown for comparison. The test cases counted along the horizontal axis represent successive runs of the PPP scheme.

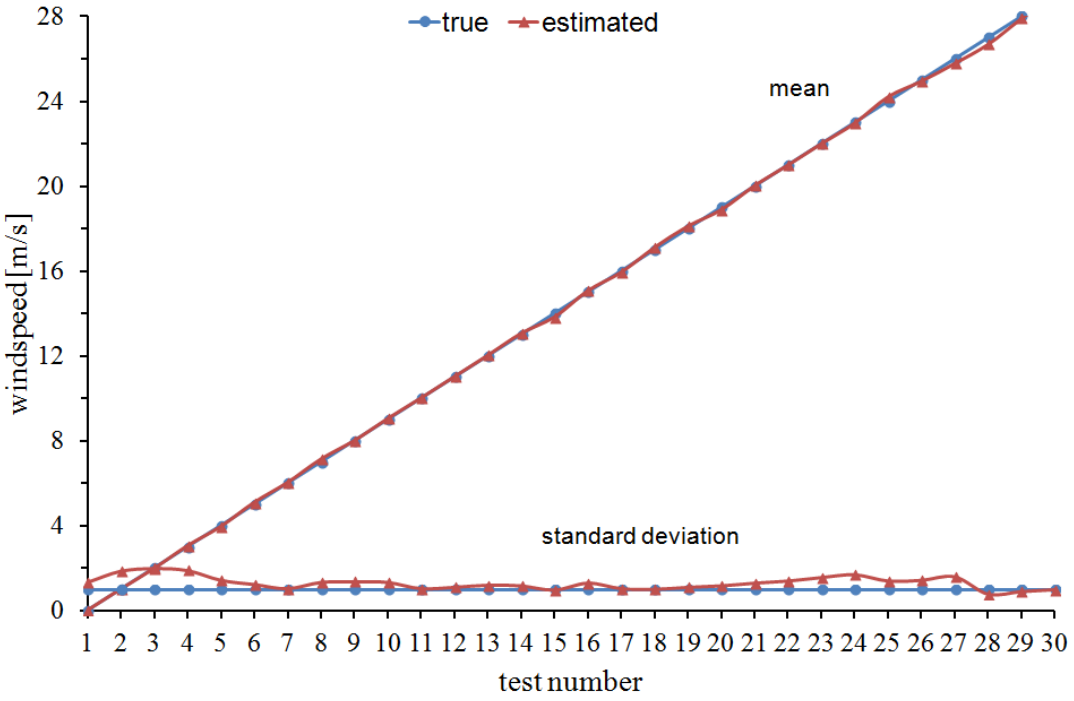

Fig. 3. Estimated mean $\tilde{v}$ and standard deviation $\tilde{\sigma}_v$, as obtained from the PPP scheme, for an input spectrum with true variance equal to 1 m^2s^{-2} and varying mean. The true values are also shown for comparison. The test cases counted along the horizontal axis represent successive runs of the PPP scheme.

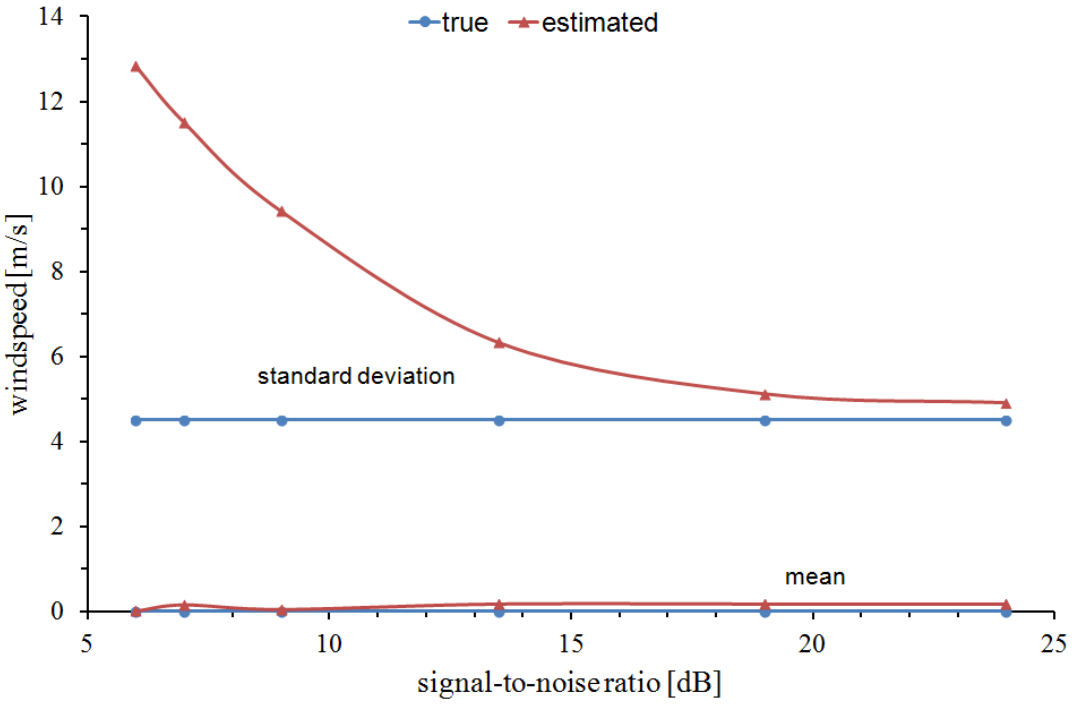

Fig. 4. Estimated mean $\tilde{v}$ and standard deviation $\tilde{\sigma}_v$, as obtained from the PPP scheme for an input spectrum with varying SNR. The true values are also shown for comparison.

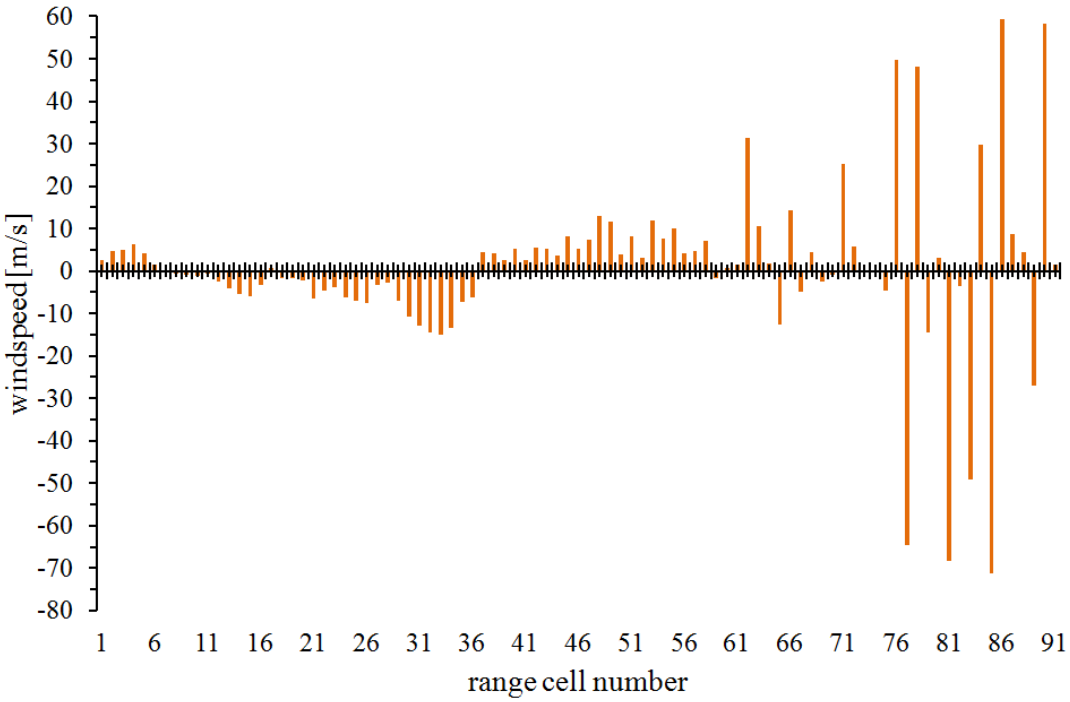

Fig. 5. Estimated mean $\tilde{v}$, as obtained from the PPP scheme, corresponding to a true windshear detected after processing of real data taken from flight experiments performed in the area of Orlando under the NASA/FAA Windshear Program. The processed data consisted of 128 IQ pairs for each of 91 range cells.